

## Summer Temperature over the Tibetan Plateau Modulated by Atlantic Multidecadal Variability

CHUNMING SHI,<sup>a</sup> CHENG SUN,<sup>a,b,k</sup> GUOCAN WU,<sup>a</sup> XIUCHEN WU,<sup>c</sup> DELIANG CHEN,<sup>d</sup>  
VALÉRIE MASSON-DELMOTTE,<sup>e</sup> JIANPING LI,<sup>a,b</sup> JIAQING XUE,<sup>f</sup> ZONGSHAN LI,<sup>g</sup> DUOYING JI,<sup>a</sup>  
JING ZHANG,<sup>a</sup> ZEXIN FAN,<sup>h</sup> MIAOGEN SHEN,<sup>i</sup> LIFU SHU,<sup>j</sup> AND PHILIPPE CIAIS<sup>e</sup>

<sup>a</sup> College of Global Change and Earth System Science, Beijing Normal University, Beijing, China

<sup>b</sup> Laboratory for Regional Oceanography and Numerical Modeling, Qingdao National Laboratory for Marine Science and Technology, Qingdao, China

<sup>c</sup> State Key Laboratory of Earth Surface Processes and Resource Ecology, Faculty of Geographical Science, Beijing Normal University, Beijing, China

<sup>d</sup> Regional Climate Group, Department of Earth Sciences, University of Gothenburg, Gothenburg, Sweden

<sup>e</sup> Laboratoire des Sciences du Climat et de l'Environnement (UMR CEA-CNRS-UVSQ 8212), Institut Pierre Simon Laplace, Gif-sur-Yvette, France

<sup>f</sup> State Key Laboratory of Numerical Modeling for Atmospheric Sciences and Geophysical Fluid Dynamics, Institute of Atmospheric Physics, Chinese Academy of Sciences, and College of Earth Science, University of Chinese Academy of Sciences, Beijing, China

<sup>g</sup> State Key Laboratory of Urban and Regional Ecology, Research Center for Eco-Environmental Sciences, Chinese Academy of Sciences, Beijing, China

<sup>h</sup> Key Laboratory of Tropical Forest Ecology, Xishuangbanna Tropical Botanical Garden, Chinese Academy of Sciences, Mengla, Mengla, Yunnan, China

<sup>i</sup> Institute of Tibetan Plateau Research, Chinese Academy of Sciences, Beijing, China


<sup>j</sup> Key Laboratory of Forest Ecology and Environment, State Forestry Administration, Institute of Forest Ecology, Environment and Protection, Chinese Academy of Forestry, Beijing, China

(Manuscript received 18 December 2017, in final form 19 March 2019)

### ABSTRACT

Rapid warming has led to an aggregated environmental degradation over the Tibetan Plateau (TP) in the last few decades, including accelerated glacier retreat, early snowmelt, permafrost degradation, and forest fire occurrence. Attribution of this warming in recent decades has mainly been focused on anthropogenic forcing. Yet, linkages to the Atlantic multidecadal variability (AMV), an essential part of the climate system causing decadal to centennial fluctuations of temperature, remains poorly understood for the TP, especially at long time scales. Using well-replicated tree-ring width records, we reconstructed 358 years of summer minimum temperature (MinT) of the whole TP. This reconstruction matches the recent warming signal recorded since the 1980s, and captures 63% of the variance in 1950–2005 instrumental records. A teleconnection from the North Atlantic to the TP is further identified based in observations and simulations with an atmospheric general circulation model (AGCM). We propose that half of the multidecadal variability of TP summer MinT can be explained by the AMV over the past three and a half centuries. Both observations and AGCM simulations indicate that the AMV warm phase induces a zonal dipole response in sea level pressure across the Atlantic–Eurasia region, with anomalously high surface pressure and corresponding downward atmospheric motion over the TP. We propose that the descending motion during warm AMV phases causes negative rainfall and positive temperature anomalies over the TP. Our findings highlight that the AMV plays a role in the multidecadal temperature variability over the TP.

---

 Denotes content that is immediately available upon publication as open access.

---

<sup>k</sup> Additional affiliation: State Key Laboratory of Satellite Ocean Environment Dynamics, Second Institute of Oceanography, Ministry of Natural Resources, Hangzhou, China.

---

Corresponding authors: Chunming Shi, chunming.shi@gmail.com; Cheng Sun, scheng@bnu.edu.cn

DOI: 10.1175/JCLI-D-17-0858.1

© 2019 American Meteorological Society. For information regarding reuse of this content and general copyright information, consult the [AMS Copyright Policy \(www.ametsoc.org/PUBSReuseLicenses\)](https://www.ametsoc.org/PUBSReuseLicenses).

## 1. Introduction

Significant global warming has been observed since the early twentieth century (Trenberth et al. 2007). Warming rates are nonuniform in latitude and altitude. High-altitude regions, such as the Tibetan Plateau (TP) (which is known as the world's "third pole" or Asia's "water tower"), are experiencing faster warming rates than other regions at the same latitude, especially in winter and spring (Liu and Chen 2000; Xie et al. 2010). The TP's warming continued during the global warming hiatus period of 1998–2013, whereas lowland areas in eastern China slightly cooled (Duan and Xiao 2015). The trend of annual mean temperature over the TP reached  $0.44^{\circ}\text{C decade}^{-1}$  in 1980–2013, which is 2–3 times above the pace recorded for the Northern Hemisphere (NH) and global mean for the same time interval (i.e.,  $0.23^{\circ}$  and  $0.16^{\circ}\text{C decade}^{-1}$ , respectively) (Duan and Xiao 2015).

The environmental impacts of recent TP warming include accelerated glacier retreat, early snowmelt, and permafrost degradation (Chen et al. 2015; Kang et al. 2010; Yao et al. 2012). Moreover, the TP warming further changed spatial-temporal patterns of monsoon precipitation (Jin and Wang 2017; Thompson et al. 2000; Yang et al. 2014), which, together with the melting of glaciers, has posed unprecedented threats to the freshwater supply as well as social and economic risks to the densely populated regions downstream (Jin and Wang 2017; Kehrwald et al. 2008; Piao et al. 2010).

The fast and persistent TP warming observed in recent decades has been attributed to increasing anthropogenic greenhouse gas forcing and snow/ice albedo feedbacks (An et al. 2016b; Liu and Chen 2000; Pepin and Lundquist 2008), especially during the global warming hiatus (You et al. 2016). This effect is further enhanced by black carbon deposition over snow and glaciers (Flanner et al. 2007). Increased absorbing aerosols, mainly black carbon, associated with biomass burning and fossil fuel consumption are ranked together as the second largest driver of Asian warming, accounting for half of the warming in some TP regions (Ramanathan et al. 2007). Altogether, most attribution studies of recent TP warming have focused on anthropogenic forcing. However, on decadal to centennial scales, the relative roles of anthropogenic forcing and natural variability remain poorly understood.

In particular, sea surface temperatures (SSTs) over the North Atlantic basin show predominant variability characterized by spatially coherent SST anomalies (Enfield et al. 2001). This variability is referred to as

Atlantic multidecadal variability (AMV), which shows an oscillatory behavior between warm and cold phases with a period of 50–70 years (Schlesinger and Ramankutty 1994; Sun et al. 2015). The AMV contributes to the multidecadal variability of the NH climate (Delworth et al. 2016; Li et al. 2013; Sun et al. 2017), especially for surface air temperatures (Knight et al. 2006; Tung and Zhou 2013; Yao et al. 2017; Zhang et al. 2007).

Potential teleconnections between AMV and TP temperature are poorly understood, due to the lack of long temperature records over the TP and the scarcity of studies assessing mechanisms linking AMV and TP climate. This motivated the development of a reliable long temperature reconstruction for the whole TP. Among existing temperature reconstructions over the TP, most are of local to regional scales (An et al. 2016a; Shi et al. 2015; Thompson et al. 1989; Tian et al. 2006; Wang et al. 2015; Yao et al. 2012). The quantitative interpretation of the  $\delta^{18}\text{O}$  signal in TP ice cores as a temperature proxy remains challenging due to the difficulty of deconvolving precipitation and temperature signals (Yao et al. 2013). Tree-ring records are useful because they are more widely distributed than glaciers, and trees at high elevations are unambiguously sensitive to growing season minimum temperature (night temperature) (Korner 1998; Rossi et al. 2008; Shi et al. 2015). With a proper detrending method, tree-ring width (TRW) is a reliable proxy for local to hemispheric temperature reconstructions decadal to multicentennial scales (Jansen et al. 2007).

This study combines 28 TRW chronologies over the TP (defined as  $27^{\circ}$ – $38^{\circ}\text{N}$ ,  $75^{\circ}$ – $103^{\circ}\text{E}$ ) which are sensitive to local summer (defined as June–August) minimum temperature (MinT), providing a reconstructed summer MinT record over the whole TP. The linkage between TP summer MinT and Atlantic SST is analyzed with instrumental and reconstructed data, and the connection mechanisms are further explored using both observations and AGCM simulations.

## 2. Materials and methods

### a. Tree-ring width data processing and screening

In this study, we compiled a dataset combining tree-ring width data of 127 sites from the International Tree Ring Data Bank and temperature reconstructions over TP (Li et al. 2012; Li et al. 2011; Shi et al. 2015). All TRW measurements were detrended with signal-free Regional Curve Standardization (sf-RCS) (Melvin and Briffa 2014a,b), the portions with EPS (expressed population signal) value less than 0.85

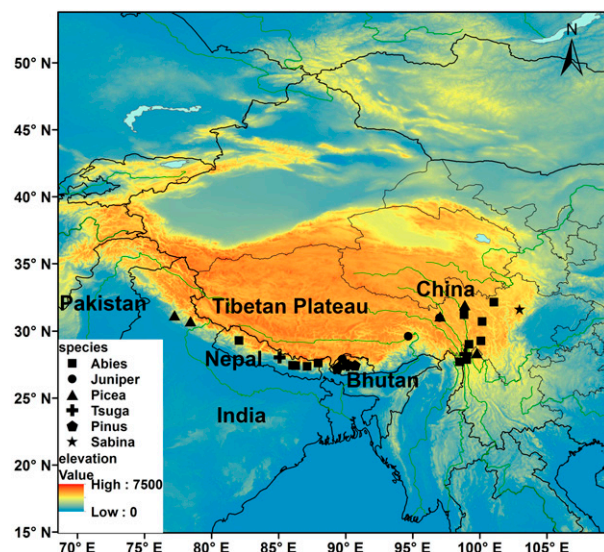


FIG. 1. Location and species of chronologies used for the TP summer minimum temperature reconstruction.

were truncated, and the number of trees in the last year of each chronology is shown in the [appendix](#) (see [Table A1](#)). Then the chronologies were Z-score normalized and linearly regressed over the maximum period of overlap with the 1950–2016 Climatic Research Unit (CRU) TS4.0 (0.5° resolution) summer (June–August) minimum temperature of the local grid point. Note that the instrumental record became available in 1950 for the TP. First, 25 TRW chronologies were selected based on their significant correlation coefficient ( $P < 0.05$ ) with CRU TS4.0 summer MinT of the local grid point ([Table A1](#)). An additional three chronologies with  $P < 0.10$  significant level were also incorporated. Therefore, a total of 28 TRW chronologies are used for our climate reconstruction ([Table A1](#)). To test the robustness of sf-RCS method for retaining temperature signal,  $P$  and  $R$  values were also calculated using high-pass filtered TRW chronologies and local CRU summer MinT data by their 20-yr loess smoothing trends ([Table A1](#)). The majority of the sampling sites were located at elevations above 3000 m above mean sea level (MSL); only four of them were located below 3000 m MSL. The TRW chronologies range between 155 and 1445 years ([Table A1](#)), with species from *Abies* (13), *Picea* (6), *Juniper* (3), *Tsuga* (3), *Pinus* (2), and *Sabina* (1) (shown in [Fig. 1](#)).

#### b. TP chronology construction and calibration with TP instrumental temperature

To test for any systematic differences in trends or variability between chronologies at contrasting elevations, we

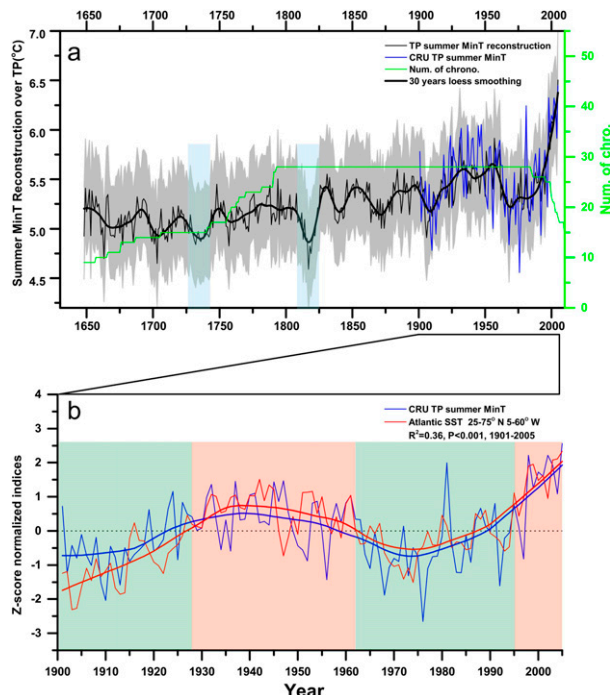


FIG. 2. (a) Instrumental (CRU TS4; blue line) and reconstructed TP (27°–38°N, 75°–103°E) summer MinT (black line). Gray shading indicates 95% confidence interval of the reconstruction. The green line is the number of chronologies, and the thick black line is the 30-yr loess smoothing. Transparent light blue bars show the two coldest epochs of the reconstruction. (b) Z-score normalized indices of CRU TP summer MinT and January–August averaged SST of Atlantic Ocean (25°–75°N, 5°–65°W; ERSST V4 dataset), green and red shadings indicate cold and warm AMV phases, and thick blue and red lines are 30-yr loess smoothing.

separated the 28 chronologies into two groups of above and below the mean elevation of 3528 m MSL and show the averages in the [appendix](#) (see [Fig. A1a](#)). Thereafter, all the 28 chronologies were averaged into one chronology referred to as the TP chronology ([Fig. A1b](#)), which shows a decreasing moving standard deviation (STD) with increasing replications. To ensure spatial coverage and reconstruction quality, only the part of chronology with STD values lower than 0.50 was retained, which is equivalent to a replication of  $N = 9$ . Then, the new TP chronology (spanning 1648–2005) was calibrated to CRU TS4.0 summer (JJA) averaged monthly MinT of TP over the period 1950–2016 using a linear regression model. The model was verified using the leave-one-out verification method over 1950–2005; this method systematically deletes one part of pair of data and derives a forecast model from the remaining data, this model was tested on the deleted data.

#### c. Reconstruction error calculation

The reconstruction errors were calculated as follows: CRU summer MinT and TP chronology were randomly



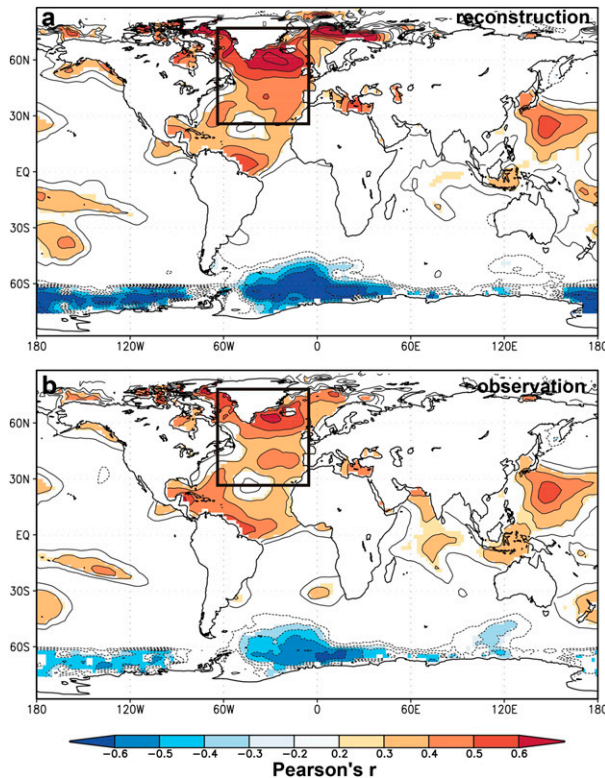


FIG. 3. Correlation coefficients of (a) reconstructed and (b) CRU TP summer MinT with January–August averaged SST (1950–2005, SST, ERSST V4 dataset). All data are linearly detrended and results are only shown where  $P < 0.05$ . Black rectangles indicate the SST region used in this study ( $25^{\circ}$ – $75^{\circ}$ N,  $5^{\circ}$ – $60^{\circ}$ W).

divided into two halves within the 1950–2005 calibration period. Each half was used to calculate a linear calibration model and validated with the other half, yielding 56 error values. The 2.5th and 97.5th percentiles of the error population after 1000 repeating were defined as a 95% confidence interval of the summer MinT reconstruction (Carré et al. 2012).

#### d. Observations of atmospheric circulation and AGCM experiments

The observed monthly mean sea level pressure (SLP) for the period 1901–2012 were obtained from NOAA's Twentieth Century Reanalysis version 2c (20CRv2c) (Compo et al. 2011). We remove the linear trends in the variables [e.g., surface air temperature (SAT) and SLP] from 1900 onward by using a linear least squares fitting method, and the aim of this procedure is to highlight the multidecadal variability superimposed upon the centennial scale trends. We conduct numerical experiments using the SPEEDY (Simplified Parameterizations, Primitive Equation Dynamics) model, which is an AGCM of intermediate

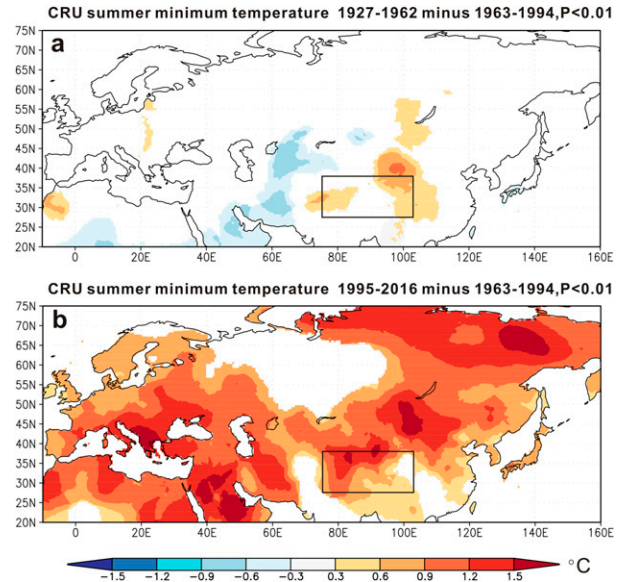


FIG. 4. Land surface CRU summer MinT anomalies corresponding to the AMV positive phases in (a) 1927–62 and (b) 1995–2016 with respect to the AMV negative phase of 1963–94 (in  $^{\circ}$ C). Rectangles show the region of the Tibetan Plateau. Results are only shown where  $P < 0.01$ .

complexity, with simplified physics and an horizontal resolution of triangular 30 ( $T30$ ;  $3.75^{\circ} \times 3.75^{\circ}$ ) with eight vertical levels (Kucharski et al. 2016). An SST-forced AGCM experiment was performed to investigate the impacts of the Atlantic SST forcing on the global atmospheric circulation. To achieve this aim, observed monthly-varying SSTs from the HadISST1 product are prescribed over the entire Atlantic basin ( $60^{\circ}$ S– $60^{\circ}$ N,  $70^{\circ}$ W– $10^{\circ}$ E); over the remaining ocean basins (i.e., Indo-Pacific basins) we prescribed observed monthly climatological SSTs (Fig. A2 in the appendix). An ensemble of five members was performed by using small initial perturbations to the atmospheric state; this experiment is referred to as ATL\_VAR\_AGCM. The model integrations start in 1872 and run to 2013. The results of the five ensemble members from the ATL\_VAR\_AGCM experiment were averaged and analyzed for the period 1900–2013.

### 3. Results

#### a. TP summer MinT reconstruction

Correlation analysis using high-pass filtered data has shown 25 out of 28 TRW chronologies are significantly (above 95% level) correlated with local CRU summer MinT (Table A1). There are 22 trees on average at the end year of chronology (Table A1). No more than

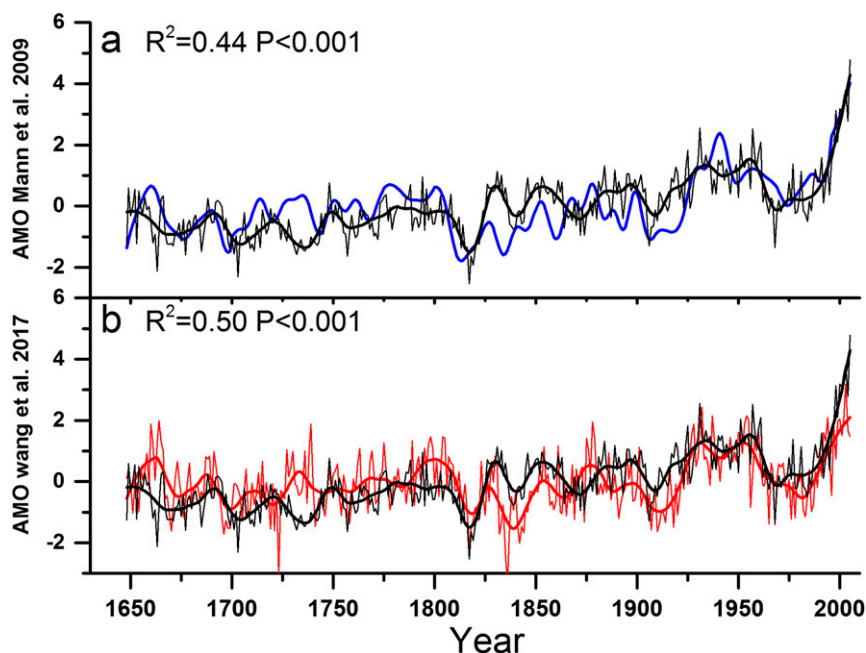


FIG. 5. Z-score normalized TP summer MinT reconstruction of this study (black line) and AMV reconstruction by (a) Mann et al. (2009) (blue line) and (b) Wang et al. (2017) (red line). The thick lines result from 30-yr loess smoothing.

12.2% of tree-ring series in any given chronology have an earliest year falling within the same 5-yr period. The robustness of the calibration was tested by both undetrended and linearly detrended TP chronologies and CRU summer MinT values (Figs. A3a,b), both showing  $R$  values above 0.7 for the central and northern TP, where published TRW data are lacking. In the eastern half,  $R$  values fall to 0.28–0.42. The  $R^2$  between TP chronology and TP ( $27^{\circ}$ – $38^{\circ}$ N,  $75^{\circ}$ – $103^{\circ}$ E) averaged summer MinT reaches 0.63 for 1950–2005 ( $R^2 = 0.57$  if linearly detrending both series) and 0.43 for 1901–2005 (Fig. A4). The RE (reduction of error statistic), CE (coefficient of efficiency), product means test (PMT), and sign test (ST) are 0.61, 0.60, 3.76, and 19.45 respectively for the leave-one-out calibration test for 1950–2005, suggesting that our TP chronology is a robust proxy for past TP summer MinT. Next, the equation of  $\text{MinT}_{\text{JJA}} = 0.65 \times \text{chronology} + 5.28$  (in  $^{\circ}\text{C}$ ), derived from the calibration of undetrended data within 1950–2005, is used to reconstruct TP summer MinT spanning 1648–2005 (Fig. 2a).

In both the instrumental record and our reconstruction, a warming phase in the 1900s to 1940s was followed by a cooling period in the 1940s to 1970s, with cold temperature anomalies in the 1970s comparable to those in the 1910s. Rapid warming is observed since the 1980s, with an accelerated rate since the 1990s. As a result, the warmest epoch of the whole reconstructed TP

temperature occurs in the 1990s to 2000s (Fig. 2a). Prior to the twentieth century, two cold intervals are reconstructed in the 1720s to 1730s and 1810s to 1820s (light blue bars in Fig. 2a). The latter follows the 1809 unknown and 1815 Tambora eruptions. The years 1816 and 2005 are associated respectively with the coldest and hottest summer MinT values in the whole record. These anomalous cold/warm intervals and multidecadal variability patterns are robust for chronology compositions above and below the mean elevation of our selected 28 chronologies (Fig. A1a).

#### b. Links between TP summer MinT and Atlantic SST

The highest correlation coefficients were found between instrumental/reconstructed TP summer MinT values and Atlantic SST averaged over January–August, suggesting that the precondition of Atlantic Ocean could modulate the following TP temperature (Figs. 3a,b respectively; 1950–2005 linearly detrended series). The CRU TP summer MinT is significantly correlated with the Atlantic SST averaged over the area used to define the AMV index ( $25^{\circ}$ – $75^{\circ}$ N,  $5^{\circ}$ – $60^{\circ}$ W;  $R^2 = 0.36$ ,  $P < 0.001$ , 1901–2005; Fig. 2b). Moreover, a wavelet coherence analysis shows that Atlantic SST and CRU TP MinT are highly coherent for periodicities of 20–30 years in the post-1950s period (Fig. A5a); the lack of coherence before the 1940s could due to the low quality of the CRU data over the TP, where extensive climate observations started since the 1950s. In

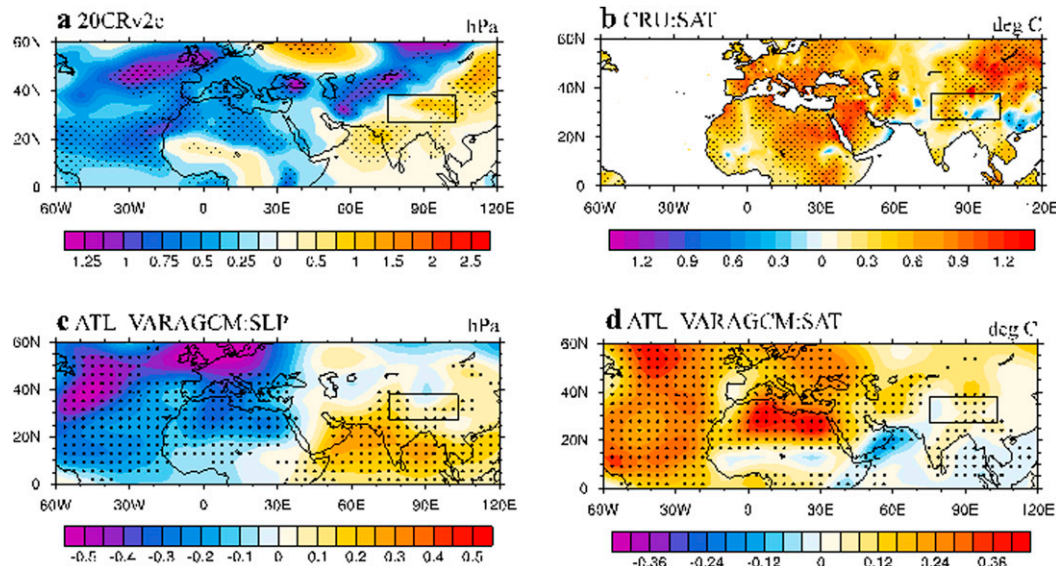


FIG. 6. (a) Differences of the JJA-mean sea level pressure (SLP; units: hPa) between the warm AMV phase 1995–2010 and the cold AMV phase 1963–94 in 20CRv2c dataset (1995–2010 minus 1963–94). (b) As in (a), but for the JJA-mean surface air temperature (SAT; units: °C) over the Eurasian continent. In (a) and (b), the long-term linear trends of SLP and SAT from 1900 onward (using a linear least squares fitting method) were removed before the composite analysis. (c) Regression map of the JJA-mean sea level pressure (SLP; units: hPa) with respect to the normalized AMV index at decadal time scales in the ATL\_VAR\_AGCM simulations. The long-term linear trend of sea level pressure for 1900–2013 was removed before the regression analysis. (d) As in (c), but for the JJA-mean surface air temperature (SAT; units: °C). Dotted shadings in (a)–(d) indicate areas above the 90% confidence level.

addition, Fig. 3 also shows that instrumental and reconstructed TP summer MinT values are strongly and negatively correlated SSTs over the Southern Ocean (with absolute  $R$  values sometimes higher than those for Atlantic SST) and positively correlated with SSTs over the north-western tropical Pacific.

In the last 100 years, warm AMV phases occurred in 1995–2005 and 1927–62, and a cold phase in 1963–94 (vertical green lines in Fig. 2b). To examine the effects of AMV phase changes on summer MinT of the entire Eurasia continent, we compare the anomalies of CRU summer MinT for the two warm AMV phases with respect to the cold one (see Figs. 4a,b for 1927–62 and 1995–2016 respectively). Despite the lower greenhouse gas forcing, the summer MinT of 1927–62 is significantly higher than that of 1963–94 over the central-western TP, the eastern TP, and north-central China (Fig. 4a;  $P < 0.01$ ). Warm anomalies of summer MinT for 1995–2016 are much larger in amplitudes and cover a greater area than those for 1927–62 (Fig. 4b), mainly due to the added effects of global warming.

The TP summer MinT reconstruction was further compared with two annual AMV reconstructions (Mann et al. 2009; Wang et al. 2017) (Figs. 5a,b). Using 30-yr smoothed series, reconstructions of TP summer MinT and AMV have been coherent at the multidecadal

scale since 1648, with an exception during the coldest interval of the 1720s to 1730s, but this interval coincides with the coldest epoch of coral-based tropical Atlantic SST reconstruction since 1552 (Saenger et al. 2009). The  $R^2$  values between 30-yr smoothed TP summer MinT reconstruction and AMV reconstructions are 0.44 and 0.50 respectively ( $P < 0.001$  in both cases), indicating that a large part of the multidecadal variability in TP summer MinT can be explained by the AMV. The coherence of TP summer MinT reconstruction with instrumental and reconstructed AMV indices is further confirmed by wavelet coherence analysis (Figs. A5b,c).

We further investigate the physical mechanism connecting the TP summer MinT and AMV using observations and atmospheric general circulation model (AGCM) simulations (see section 2 for details). The difference of observed sea level pressure (SLP) and JJA-mean surface air temperature anomalies between the warm and cold AMV phases is shown in Figs. 6a and 6b, respectively. The SLP anomalies mainly show an east–west dipole pattern across the Atlantic–Eurasia region with positive (anticyclonic) anomalies over South and East Asia and negative anomalies over the North Atlantic. Significant high-pressure anomalies are observed over the TP region during warm AMV phase.



TABLE A1. Detailed information of TRW chronologies used in this study: latitude, longitude, species, elevation, correlation coefficient with CRU summer minimum temperature at the local grid point ( $R$ ), and corresponding  $P$  value;  $R_d$  and  $P_d$  are  $P$  and  $R$  values calculated with TRW chronologies and summer minimum temperature data high-pass filtered by their 20-yr loess smoothing trends, start and end year of each chronology with EPS value above 0.85, and number of trees at the end of the year.

ID	Lat (°N)	Lon (°E)	Species	Elev (m)	$R$	$P$	$R_d$	$P_d$	Start	End	No. of trees at end of year
BT005	27.45	90.15	<i>Tsuga</i>	3392	0.29	0.03	0.31	0.02	1735	2006	7
BT006	27.47	89.5	<i>Picea</i>	3505	0.38	0.00	0.37	0.00	1539	2005	14
BT012	27.45	90.7	<i>Pinus</i>	3440	0.26	0.05	0.33	0.01	1681	2003	36
BT013	27.25	89.38	<i>Pinus</i>	2412	0.57	0.00	0.58	0.00	1817	2005	8
BT019	27.92	89.75	<i>Juniper</i>	3352	0.45	0.00	0.28	0.03	1757	2006	14
BT020	27.45	90.15	<i>Abies</i>	3392	0.33	0.01	0.41	0.00	1753	2006	7
CHIN018	29.28	100.08	<i>Abies</i>	4150	0.25	0.07	0.26	0.05	1615	2006	57
CHIN042	31.95	98.87	<i>Picea</i>	4098	0.24	0.10	0.24	0.10	1617	1996	13
CHIN045	29.62	94.67	<i>Juniper</i>	4480	0.31	0.04	0.29	0.05	1642	2003	12
CHIN047	31.12	97.03	<i>Picea</i>	4081	0.36	0.01	0.29	0.06	1636	2005	20
CHIN074	31	97	<i>Juniper</i>	4450	0.32	0.01	0.32	0.01	565	2010	23
INDI016	31.2	77.23	<i>Picea</i>	3000	0.42	0.01	0.42	0.01	1776	1989	10
INDI019	30.75	78.42	<i>Picea</i>	2400	0.34	0.04	0.34	0.03	1835	1990	10
NEPA009	27.43	86.28	<i>Abies</i>	3600	0.33	0.02	0.35	0.01	1651	1998	25
NEPA020	29.3	82.05	<i>Abies</i>	3450	0.36	0.05	0.35	0.06	1751	1979	20
NEPA021	27.63	87.95	<i>Abies</i>	3740	0.46	0.00	0.43	0.00	1660	1999	35
NEPA022	27.45	86.05	<i>Abies</i>	3720	0.42	0.02	0.41	0.03	1738	1978	8
NEPA026	27.38	87.13	<i>Abies</i>	2900	0.27	0.08	0.31	0.04	1785	1993	10
NEPA039	28.03	85.07	<i>Tsuga</i>	3115	0.29	0.05	0.27	0.06	1750	1996	18
YL	28.27	98.93	<i>Tsuga</i>	3150	0.40	0.00	0.26	0.05	1759	2005	32
BD	27.88	99.03	<i>Abies</i>	3300	0.46	0.00	0.30	0.02	1670	2005	31
GS	27.72	98.5	<i>Abies</i>	2600	0.35	0.01	0.30	0.02	1640	2005	15
DR	29.02	99.201	<i>Abies</i>	4221	0.51	0.00	0.35	0.01	1700	2011	35
XL	30.73	100.17	<i>Abies</i>	3522	0.30	0.00	0.41	0.00	1764	2012	31
DF	32.17	101.05	<i>Abies</i>	4113	0.36	0.00	0.40	0.00	1785	2012	34
BY	31.24	98.83	<i>Abies</i>	4012	0.44	0.00	0.41	0.00	1787	2012	37
MYL	31.63	102.96	<i>Sabina</i>	3750	0.57	0.00	0.51	0.00	1785	2009	23
GZ	28.37	99.77	<i>Picea</i>	3444	0.45	0.00	0.26	0.05	1475	2003	25

We also examined the SLP anomaly patterns using several other atmospheric reanalysis datasets (i.e., NCEP and ERA-20C), which are shown in Fig. A6. The main structures of the AMO-related SLP pattern are consistent throughout different atmospheric reanalysis datasets, showing a zonal dipole structure across the Atlantic–Eurasia region. Nevertheless, it is noted that in 20CR2 and ERA-20C the SLP anomalies over tropical North Atlantic and southern Asia are stronger than the NCEP dataset.

The simulated responses of summertime SLP and surface air temperature to the AMV forcing are further examined using an AGCM stand-alone pacemaker experiment forced by the observed monthly-varying Atlantic SST and climatological Indo-Pacific SST using the SPEEDY AGCM (see section 2 for details). The results are shown in Figs. 6c and 6d. In response to the AMV forcing, the simulated SLP anomalies generally resemble observations, showing a clear zonal dipole structure with high SLP anomalies east of 30°E and low SLP anomalies west of 30°E, with some differences in Arabian Peninsula and northern China. The simulated SAT anomalies

associated with the warm AMV phase show a continental-scale warm pattern across Eurasia, which is in accord with the observed anomalies (Fig. 4).

The zonal dipole pattern of SLP anomalies associated with the AMV is crucial for understanding the remote impact of AMV on summer TP SAT. In response to the warm AMV phase, the SLP field shows strong anomalous low pressure over the North Atlantic region, resulting from the anomalous ascending motion generated by the warm AMV SST anomaly in this region. In contrast, anomalous surface high pressure prevails over South and East Asia during the warm AMV phase. These downstream remote responses of atmospheric circulation to North Atlantic SST can be physically interpreted. It can be reasonably speculated that the warm SST anomaly in the North Atlantic may give rise to strong upward motion and upper-level divergence, and the corresponding outflow heads eastward and converges over South and East Asia, further inducing a compensating subsidence and an anomalous high in that region.

Previous modeling studies have suggested that the tropical Atlantic SST forcing can generate a

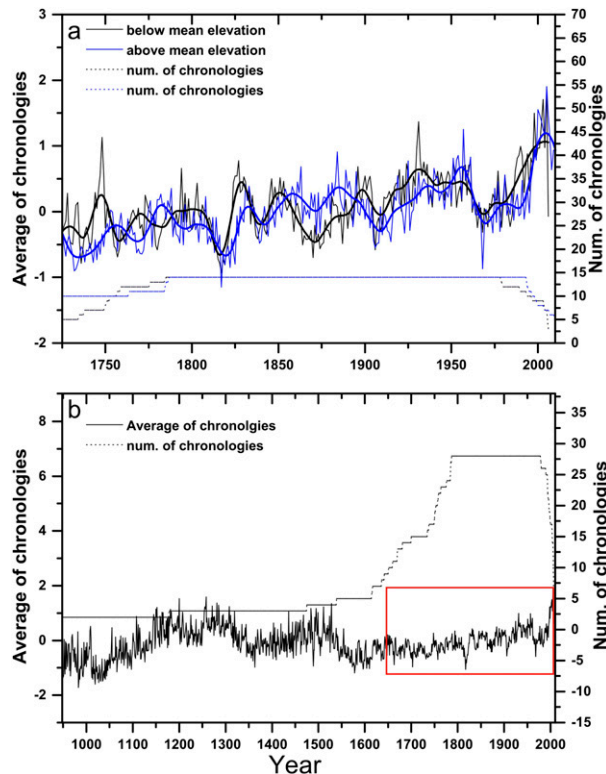


FIG. A1. Chronology compositions for above and below mean elevation and their 30-yr loess smoothing (blue and black lines respectively). (a) Horizontal dotted lines are the number of chronologies for each composition. (b) Average of all chronologies and replication number, red box indicates the interval used for TP MinT reconstruction.

Gill–Matsuno-type response of atmospheric circulation (i.e., a Kelvin wave propagating to the east and a Rossby wave to the west of the heating), characterized by a low-level anomalous low over the tropical Atlantic and a high over South Asia and the Indian Ocean, explaining the interannual teleconnection of the tropical Atlantic to the Indian summer monsoon (Kucharski et al. 2009; Wang et al. 2009). Both observations and simulations reveal that, at multidecadal time scales, SLP anomalies show zonal dipole responses to the Atlantic SST forcing, supporting a dynamical Gill–Matsuno-type response.

Consistent with the zonal dipole of SLP anomalies, the simulated summer rainfall across the Atlantic–Eurasia region also exhibits a dipole-like pattern in response to the AMV SST forcing (Fig. A7). Warm AMV phases lead to wet anomalies over the North Atlantic and adjacent continents, and dry anomalies over parts of South and East Asia, including the TP, where the descent-induced adiabatic warming may contribute to the warm SAT anomaly. The dry anomalies over the TP region during warm AMV periods

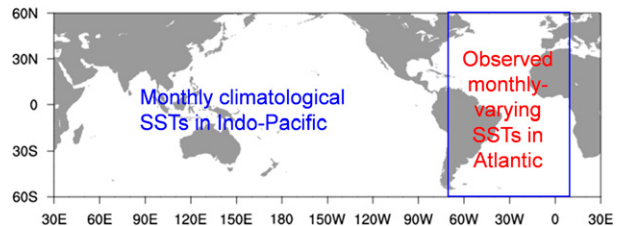


FIG. A2. Schematic graph for the prescribed bottom boundary condition in the SST forced AGCM experiment ATL\_VAR\_AGCM.

may favor enhanced incoming solar radiation and reduced surface evapotranspiration (Trenberth and Shea 2005; van der Ent et al. 2010), further leading to the warm SAT anomaly in summer through land–atmosphere feedbacks.

However, more work is still needed to fully explore the potential mechanisms connecting the multidecadal North Atlantic SST variability and summer temperatures on the TP. While the changes in SLP, SAT, and rainfall identified in observations and the AGCM simulations in this study identified a clear link between North Atlantic SSTs and SLP over South Asia, they only hint at a possible dynamical mechanism. The Gill–Matsuno-type dynamical response to North Atlantic heating needs to be further tested and validated. In addition, the links between the large-scale atmospheric circulation response and surface temperatures over the TP also require further investigation.

#### 4. Discussion

The unprecedented increase in the last decades of TP chronology is not likely due to a sharp decreased sample replication, since there are still an abundant number of trees at the end year of the 28 chronologies. The high coherence of high-pass filtered TRW chronologies and local summer MinT could suggest moderate non-climate-related signal remaining in the TRW chronologies. By pooling 28 chronologies spreading all over the TP, we believe the site-specific nonclimatic signals could be further removed, and the relationship between TP chronology and temperature is strengthened as chronologies are aggregated.

Atlantic circulation is a major source of natural variability of Northern Hemisphere climate (Delworth et al. 2016), including multidecadal variations in NH temperature (Knight et al. 2006; Tung and Zhou 2013; Zhang et al. 2007). We report that the negative AMV phase during 1963–94 offsets the greenhouse forcing–induced warming trends for the entire TP, leading to anomalous cold summer conditions during this epoch. In fact, the TP is one of the few regions over Eurasia where summer MinT values reflect AMV phase alternations over 1927–94. In 1995–2016, CRU



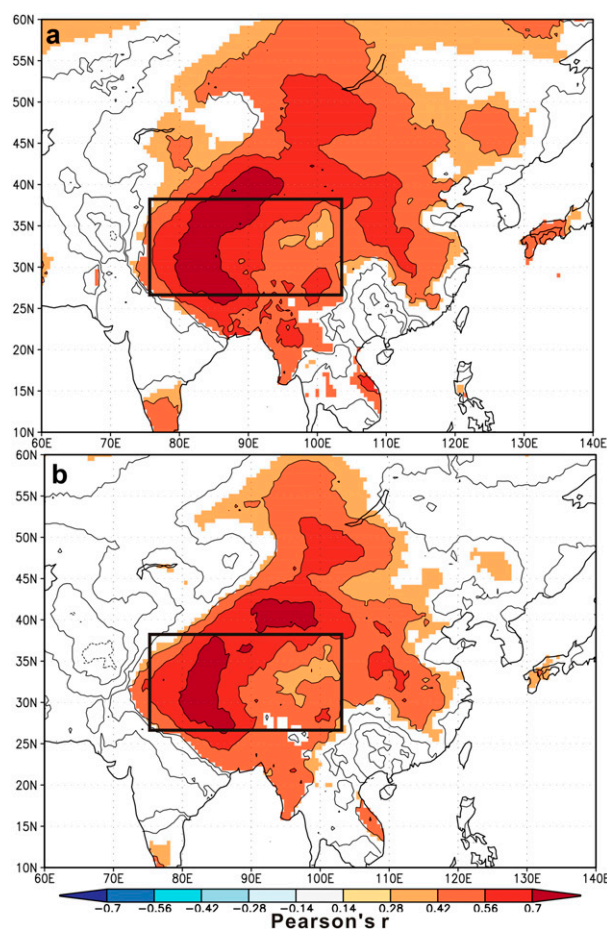


FIG. A3. (a) Spatial correlation coefficients of the TP chronology and 1950–2005 CRU TS4 summer MinT. (b) As in (a), but using linear detrended data. Results are only shown where  $P < 0.01$ . Black rectangles show the TP region defined in this study.

summer MinT values are higher than those of 1963–94 for most regions of Eurasia. Since the mid-1990s, the positive AMV phase has amplified summer warming of Eurasia caused by anthropogenic forcing (Zhang et al. 2007). This mechanism could also explain the unprecedented warm period observed in the TP summer MinT since the 1990s. However, an increased anthropogenic global warming signal of the last decades could be solely responsible for the unprecedented warming. While a quantitative attribution of warming trends to AMV versus anthropogenic forcing is outside the scope of this study, our findings suggest that both the AMV phase and anthropogenic forcing need to be considered when predicting future TP decadal temperature variations.

The trend of instrumental TP summer MinT closely follows that of Atlantic SST, which represents a combination of greenhouse gas-induced warming and internal variability within the Atlantic Ocean. The TP

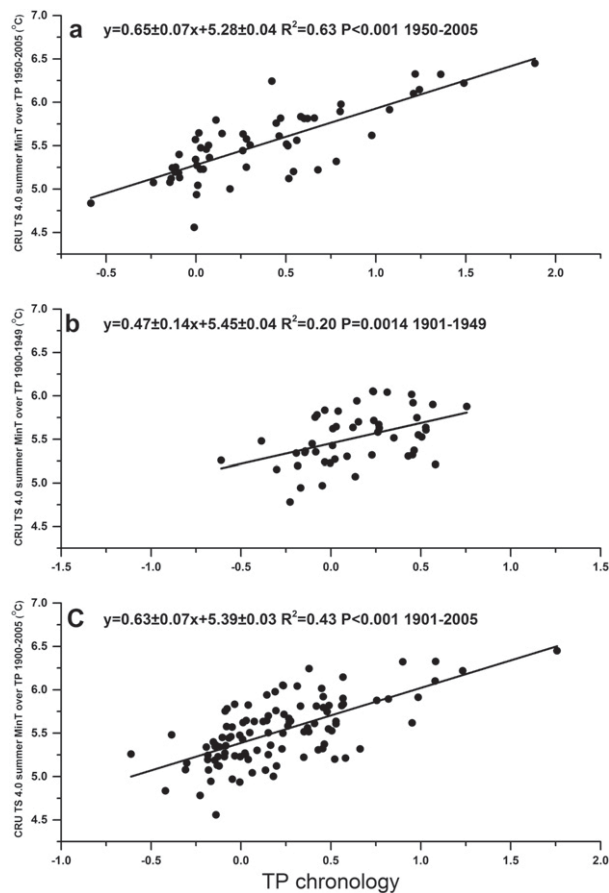


FIG. A4. Calibration of the TP chronology with CRU TS4 TP ( $27^{\circ}$ – $38^{\circ}$ N,  $75^{\circ}$ – $103^{\circ}$ E) summer MinT for periods (a) 1950–2005, (b) 1901–49, and (c) 1901–2005. All data used in this figure are not detrended.

summer MinT anomaly of 1995–2016 is not unique compared with many other regions of Eurasia. Signals of extra warming contributors, such as snow albedo and absorbing aerosols, are likely absent in our sampling sites for summer season, as the warming trends of TP are asymmetrical across seasons, with the largest warming trend in spring and winter (Liu et al. 2006, 2009; You et al. 2008). TP forest stands are far below glaciers and the  $0^{\circ}$ C isotherm where positive feedback of snow albedo is significant. The warming effect of absorbing aerosols is prominent in west TP and Himalaya regions in late spring (Gautam et al. 2009; Lau et al. 2010) and may have a weak connection with summer minimum temperature (Korner 1998; Rossi et al. 2008).

However, considerable uncertainties may still exist in the observations, simulations, and diagnostics presented in this study. There is a severe lack of instrumental records prior to the 1950s over the TP, especially for the surface pressure field (Moore 2012; Liu and Chen 2000; You et al. 2017). Although there are several reanalysis

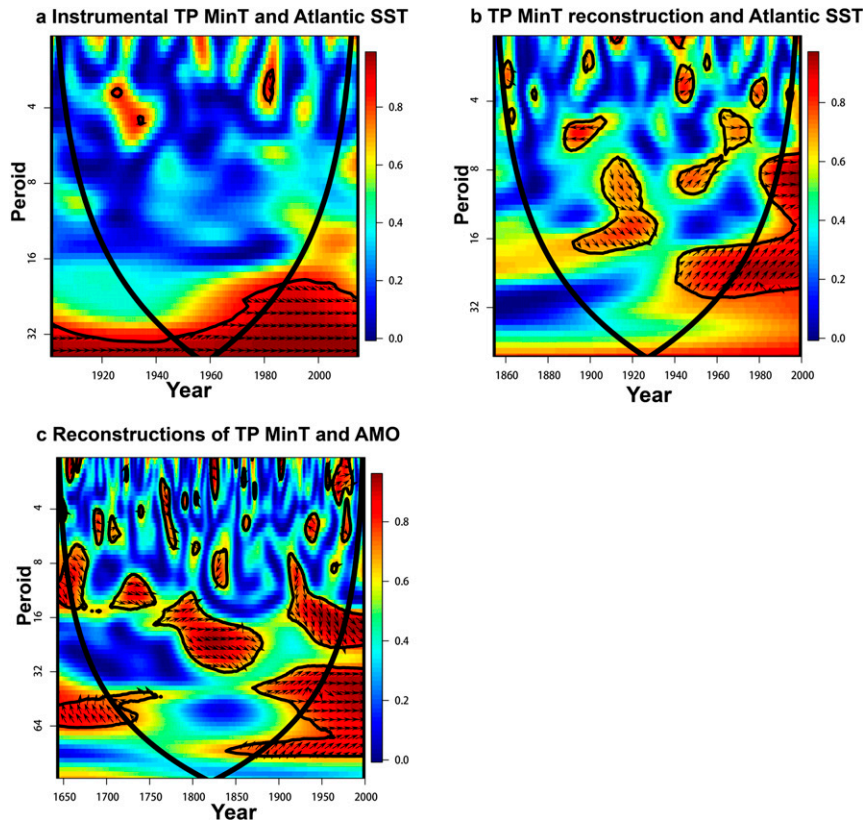


FIG. A5. (a) Wavelet coherence (WTC) of CRU TP summer MinT with January–August averaged North Atlantic SST (ERSST V4 dataset), (b) TP summer MinT reconstruction with January–August averaged North Atlantic SST, and (c) TP summer MinT reconstruction with annual AMV reconstruction by Wang et al. (2017). Calculations were performed using R language with the “biwavelet” package. Black contours are significantly coherent at the 95% level. Arrows pointing to the right mean summer MinT and SST/AMV are in phase; arrows pointing up mean that SST/AMV lead summer MinT by  $\pi/2$ . The cone of influence (white lines) designates the area affected by edge effects. In the area inside the cone, edge effects can be neglected. For the AMV reconstruction of Mann et al. (2009) only smoothed data are available; as a result, no WTC analysis is feasible.

datasets that span throughout the twentieth century (e.g., 20CR and ERA-20C), these products are based on the assimilation of observational surface pressure. Thus, the lack of observations of surface pressure over TP makes these products unreliable over the TP for the first half of the twentieth century. A limitation of the AGCM simulations is that we only consider the SST forcing confined over the Atlantic basin, and the influences of other basins on the TP multidecadal variability should be investigated and compared with the Atlantic basin in the future. Additional uncertainties could also arise from inhomogeneous distribution of the sampling sites, varying time spans of the TRW records, and interpretations of the correlations and mechanisms linking TP MinT and AMV. We suggest that more temperature reconstructions based on tree rings and other paleoclimate

proxies over the central and northern TP are still needed to test our results.

## 5. Conclusions

Teleconnection between the AMV and TP is supported by statistical analyses of observations, temperature reconstruction spanning the last several centuries, and AGCM modeling. Although speculative, the AMV warm phase may induce a zonal dipole response of atmospheric circulation with an anomalous surface high and large-scale subsidence over Southeast Asia and the TP region. This anomalous descending motion leads to drying and surface air temperature warming. We conclude that the variability in TP summer MinT has been modulated by the AMV since 1648. Our results

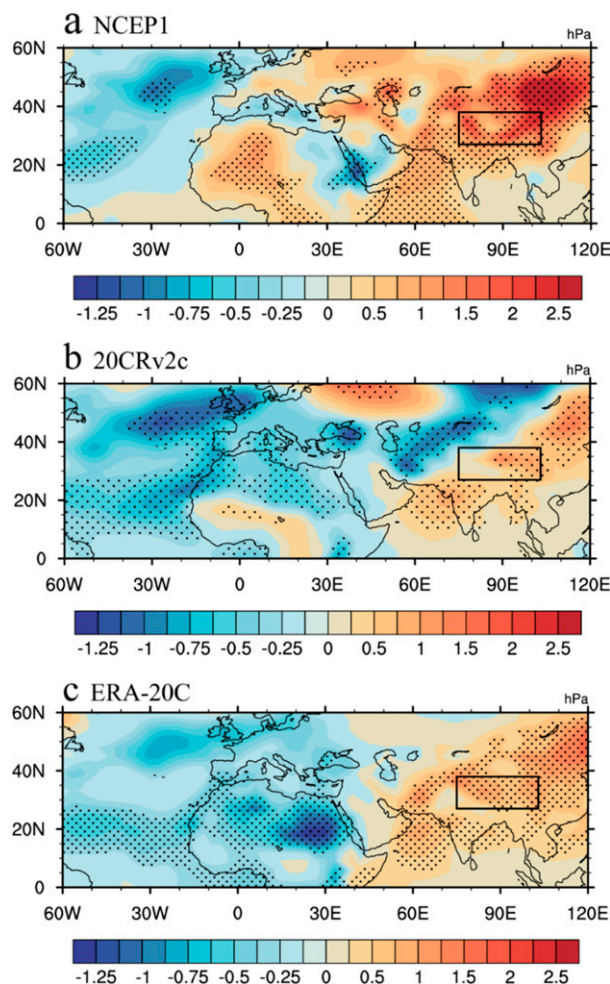


FIG. A6. (a) Composite differences of the JJA-mean sea level pressure (units: hPa) between the warm AMV phase and the cold phase in NCEP dataset (1995–2010 minus 1963–94). (b), (c) As in (a), but for the 20CR2 and ERA-20C datasets, respectively. The effect of global SST warming trend (regressions to the linear warming trend using a linear least squares fitting method) was removed from the SLP anomalies before we performed the composite analysis.

suggest a broad impact of AMV on Eurasian climate. Further investigations are needed to fully understand the teleconnection from Atlantic SST to Eurasian surface temperature and to incorporate this information for regional decadal prediction.

**Acknowledgments.** This study was supported by the National Key Research and Development Plan (2017YFD0600106), the National Natural Science Foundation of China (31600354, 31570645 and 41775038), and the Fundamental Research Funds for the Central Universities. C.S. is supported by the open fund of State Key Laboratory of Satellite Ocean Environment Dynamics, Second Institute of Oceanography, MNR (QNHX1919).

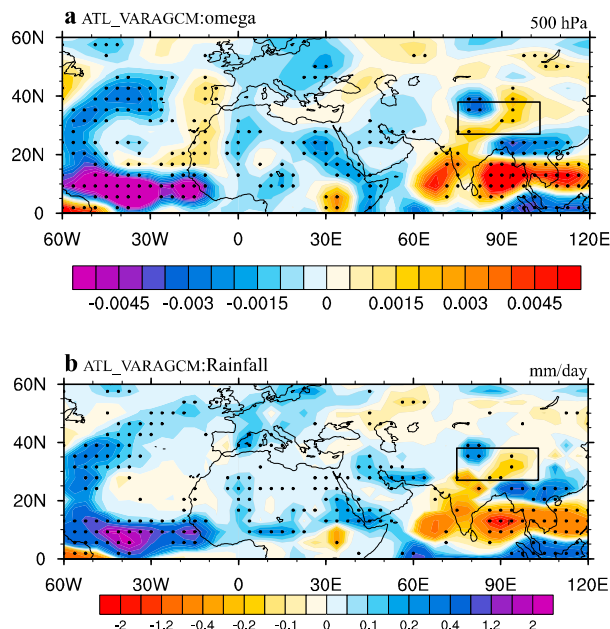


FIG. A7. Regressions of JJA-mean (a) vertical velocity (units:  $10^{-2} \text{ Pa s}^{-1}$ ) and (b) rainfall (units:  $\text{mm day}^{-1}$ ) onto the normalized AMV index at decadal time scales in the ATL\_VAR\_AGCM simulations. Dotted shadings denote regressions significant at the 90% confidence level. The long-term linear trends for 1900–2013 in both variables were removed before the regression analyses.

## APPENDIX

### Additional Analyses

Detailed information about the sampling sites, chronology composition, bottom boundary condition of the SST-forced AGCM experiment, spatial correlation and linear calibration between the TP chronology and summer MinT, wavelet coherence analysis, composite differences of the sea level pressure, and regressions of vertical velocity and rainfall onto the AMV index are provided in Table A1 and Figs. A1–A7.

## REFERENCES

- An, W., S. Hou, W. Zhang, Y. Wang, Y. Liu, S. Wu, and H. Pang, 2016a: Significant recent warming over the northern Tibetan Plateau from ice core  $\delta^{18}\text{O}$  records. *Climate Past*, **12**, 201–211, <https://doi.org/10.5194/cp-12-201-2016>.
- , —, —, S. Wu, H. Xu, H. Pang, Y. Wang, and Y. Liu, 2016b: Possible recent warming hiatus on the northwestern Tibetan Plateau derived from ice core records. *Sci. Rep.*, **6**, 32813, <https://doi.org/10.1038/srep32813>.
- Carré, M., J. P. Sachs, J. M. Wallace, and C. Favier, 2012: Exploring errors in paleoclimate proxy reconstructions using Monte Carlo simulations: Paleotemperature from mollusk and coral geochemistry. *Climate Past*, **8**, 433–450, <https://doi.org/10.5194/cp-8-433-2012>.



- Chen, D., and Coauthors, 2015: Assessment of past, present and future environmental changes on the Tibetan Plateau (in Chinese with English abstract). *Chin. Sci. Bull.*, **60**, 3025–3035, <https://doi.org/10.1360/n972014-01370>.
- Compo, G. P., and Coauthors, 2011: The Twentieth Century Reanalysis Project. *Quart. J. Roy. Meteor. Soc.*, **137**, 1–28, <https://doi.org/doi:10.1002/qj.776>.
- Delworth, T. L., F. Zeng, G. A. Vecchi, X. Yang, L. Zhang, and R. Zhang, 2016: The North Atlantic Oscillation as a driver of rapid climate change in the Northern Hemisphere. *Nat. Geosci.*, **9**, 509–512, <https://doi.org/10.1038/ngeo2738>.
- Duan, A., and Z. Xiao, 2015: Does the climate warming hiatus exist over the Tibetan Plateau? *Sci. Rep.*, **5**, 13711, <https://doi.org/10.1038/srep13711>.
- Enfield, D. B., A. M. Mestas-Núñez, and P. J. Trimble, 2001: The Atlantic multidecadal oscillation and its relation to rainfall and river flows in the continental U.S. *Geophys. Res. Lett.*, **28**, 2077–2080, <https://doi.org/10.1029/2000GL012745>.
- Flanner, M. G., C. S. Zender, J. T. Randerson, and P. J. Rasch, 2007: Present-day climate forcing and response from black carbon in snow. *J. Geophys. Res.*, **112**, D11202, <https://doi.org/10.1029/2006JD008003>.
- Gautam, R., N. C. Hsu, K. M. Lau, S. C. Tsay, and M. Kafatos, 2009: Enhanced pre-monsoon warming over the Himalayan-Gangetic region from 1979 to 2007. *Geophys. Res. Lett.*, **36**, L07704, <https://doi.org/10.1029/2009GL037641>.
- Jansen, E., and Coauthors, 2007: Palaeoclimate. *Climate Change 2007: The Physical Science Basis*, S. Solomon et al., Eds., Cambridge University Press, 433–497.
- Jin, Q., and C. Wang, 2017: A revival of Indian summer monsoon rainfall since 2002. *Nat. Climate Change*, **7**, 587–594, <https://doi.org/10.1038/nclimate3348>.
- Kang, S., Y. Xu, Q. You, W.-A. Flügel, N. Pepin, and T. Yao, 2010: Review of climate and cryospheric change in the Tibetan Plateau. *Environ. Res. Lett.*, **5**, 015101, <https://doi.org/10.1088/1748-9326/5/1/015101>.
- Kehrwald, N. M., and Coauthors, 2008: Mass loss on Himalayan glacier endangers water resources. *Geophys. Res. Lett.*, **35**, L22503, <https://doi.org/10.1029/2008GL035556>.
- Knight, J. R., C. K. Folland, and A. A. Scaife, 2006: Climate impacts of the Atlantic Multidecadal Oscillation. *Geophys. Res. Lett.*, **33**, L17706, <https://doi.org/10.1029/2006GL026242>.
- Korner, C., 1998: A re-assessment of high elevation treeline positions and their explanation. *Oecologia*, **115**, 445–459, <https://doi.org/10.1007/s004420050540>.
- Kucharski, F., A. Bracco, J. H. Yoo, A. M. Tompkins, L. Feudale, P. Ruti, and A. Dell'Aquila, 2009: A Gill-Matsuno-type mechanism explains the tropical Atlantic influence on African and Indian monsoon rainfall. *Quart. J. Roy. Meteor. Soc.*, **135**, 569–579, <https://doi.org/10.1002/qj.406>.
- , and Coauthors, 2016: The teleconnection of the tropical Atlantic to Indo-Pacific sea surface temperatures on interannual to centennial time scales: A review of recent findings. *Atmosphere*, **7**, 29, <https://doi.org/10.3390/atmos7020029>.
- Lau, W. K. M., M.-K. Kim, K.-M. Kim, and W.-S. Lee, 2010: Enhanced surface warming and accelerated snow melt in the Himalayas and Tibetan Plateau induced by absorbing aerosols. *Environ. Res. Lett.*, **5**, 025204, <https://doi.org/10.1088/1748-9326/5/2/025204>.
- Li, J., C. Sun, and F.-F. Jin, 2013: NAO implicated as a predictor of Northern Hemisphere mean temperature multidecadal variability. *Geophys. Res. Lett.*, **40**, 5497–5502, <https://doi.org/10.1002/2013GL057877>.
- Li, Z., C. M. Shi, Y. Liu, J. Zhang, Q. Zhang, and K. Ma, 2011: Summer mean temperature variation from 1710–2005 inferred from tree-ring data of the Baimang Snow Mountains, northwestern Yunnan, China. *Climate Res.*, **47**, 207–218, <https://doi.org/10.3354/cr01012>.
- , Q. Zhang, and K. Ma, 2012: Tree-ring reconstruction of summer temperature for A.D. 1475–2003 in the central Hengduan Mountains, Northwestern Yunnan, China. *Climatic Change*, **110**, 455–467, <https://doi.org/10.1007/s10584-011-0111-z>.
- Liu, X., and B. Chen, 2000: Climatic warming in the Tibetan Plateau during recent decades. *Int. J. Climatol.*, **20**, 1729–1742, [https://doi.org/10.1002/1097-0088\(20001130\)20:14<1729::AID-JOC556>3.0.CO;2-Y](https://doi.org/10.1002/1097-0088(20001130)20:14<1729::AID-JOC556>3.0.CO;2-Y).
- , Z.-Y. Yin, X. Shao, and N. Qin, 2006: Temporal trends and variability of daily maximum and minimum, extreme temperature events, and growing season length over the eastern and central Tibetan Plateau during 1961–2003. *J. Geophys. Res.*, **111**, D19109, <https://doi.org/10.1029/2005JD006915>.
- , Z. Cheng, L. Yan, and Z.-Y. Yin, 2009: Elevation dependency of recent and future minimum surface air temperature trends in the Tibetan Plateau and its surroundings. *Global Planet. Change*, **68**, 164–174, <https://doi.org/10.1016/j.gloplacha.2009.03.017>.
- Mann, M. E., and Coauthors, 2009: Global signatures and dynamical origins of the Little Ice Age and medieval climate anomaly. *Science*, **326**, 1256–1260, <https://doi.org/10.1126/science.1177303>.
- Melvin, T. M., and K. R. Briffa, 2014a: CRUST: Software for the implementation of Regional Chronology Standardisation: Part 1. Signal-free RCS. *Dendrochronologia*, **32**, 7–20, <https://doi.org/10.1016/j.dendro.2013.06.002>.
- , and —, 2014b: CRUST: Software for the implementation of Regional Chronology Standardisation: Part 2. Further RCS options and recommendations. *Dendrochronologia*, **32**, 343–356, <https://doi.org/10.1016/j.dendro.2014.07.008>.
- Moore, G. W. K., 2012: Surface pressure record of Tibetan Plateau warming since the 1870s. *Quart. J. Roy. Meteor. Soc.*, **138**, 1999–2008, <https://doi.org/10.1002/qj.1948>.
- Pepin, N. C., and J. D. Lundquist, 2008: Temperature trends at high elevations: Patterns across the globe. *Geophys. Res. Lett.*, **35**, L14701, <https://doi.org/10.1029/2008GL034026>.
- Piao, S. L., and Coauthors, 2010: The impacts of climate change on water resources and agriculture in China. *Nature*, **467**, 43–51, <https://doi.org/10.1038/nature09364>.
- Ramanathan, V., M. V. Ramana, G. Roberts, D. Kim, C. Corrigan, C. Chung, and D. Winker, 2007: Warming trends in Asia amplified by brown cloud solar absorption. *Nature*, **448**, 575–578, <https://doi.org/10.1038/nature06019>.
- Rossi, S., and Coauthors, 2008: Critical temperatures for xylogenesis in conifers of cold climates. *Global Ecol. Biogeogr.*, **17**, 696–707, <https://doi.org/10.1111/j.1466-8238.2008.00417.x>.
- Saenger, C., A. L. Cohen, D. W. Oppo, R. B. Halley, and J. E. Carilli, 2009: Surface-temperature trends and variability in the low-latitude North Atlantic since 1552. *Nat. Geosci.*, **2**, 492–495, <https://doi.org/10.1038/ngeo552>.
- Schlesinger, M. E., and N. Ramankutty, 1994: An oscillation in the global climate system of period 65–70 years. *Nature*, **367**, 723–726, <https://doi.org/10.1038/367723a0>.
- Shi, C., V. Masson-Delmotte, V. Daux, Z. Li, M. Carré, and J. C. Moore, 2015: Unprecedented recent warming rate and temperature variability over the east Tibetan Plateau inferred



- from Alpine treeline dendrochronology. *Climate Dyn.*, **45**, 1367–1380, <https://doi.org/10.1007/s00382-014-2386-z>.
- Sun, C., J. Li, and F.-F. Jin, 2015: A delayed oscillator model for the quasi-periodic multidecadal variability of the NAO. *Climate Dyn.*, **45**, 2083–2099, <https://doi.org/10.1007/s00382-014-2459-z>.
- , F. Kucharski, J. Li, F.-F. Jin, I.-S. Kang, and R. Ding, 2017: Western tropical Pacific multidecadal variability forced by the Atlantic multidecadal oscillation. *Nat. Commun.*, **8**, 15998, <https://doi.org/10.1038/ncomms15998>.
- Tandong, Y., K. Duan, B. Xu, N. Wang, J. Pu, S. Kang, X. Qin, and L. G. Thompson, 2002: Temperature and methane changes over the past 1000 years recorded in Dasuopu glacier (central Himalaya) ice core. *Ann. Glaciol.*, **35**, 379–383, <https://doi.org/10.3189/172756402781816997>.
- Thompson, L. G., and Coauthors, 1989: Holocene–late Pleistocene climatic ice core records from Qinghai–Tibetan Plateau. *Science*, **246**, 474–477, <https://doi.org/10.1126/science.246.4929.474>.
- , T. Yao, E. Mosley-Thompson, M. E. Davis, K. A. Henderson, and P.-N. Lin, 2000: A high-resolution millennial record of the South Asian monsoon from Himalayan ice cores. *Science*, **289**, 1916–1919, <https://doi.org/10.1126/science.289.5486.1916>.
- Tian, L., and Coauthors, 2006: Recent rapid warming trend revealed from the isotopic record in Muztagata ice core, eastern Pamirs. *J. Geophys. Res.*, **111**, D13103, <https://doi.org/10.1029/2005JD006249>.
- Trenberth, K. E., and D. J. Shea, 2005: Relationships between precipitation and surface temperature. *Geophys. Res. Lett.*, **32**, L14703, <https://doi.org/10.1029/2005GL022760>.
- , and Coauthors, 2007: Observations: Surface and atmospheric climate change. *Climate Change 2007: The Physical Science Basis*, S. Solomon et al., Eds., Cambridge University Press, 235–336.
- Tung, K.-K., and J. Zhou, 2013: Using data to attribute episodes of warming and cooling in instrumental records. *Proc. Natl. Acad. Sci. USA*, **110**, 2058–2063, <https://doi.org/10.1073/pnas.1212471110>.
- van der Ent, R. J., H. H. G. Savenije, B. Schaefli, and S. C. Steele-Dunne, 2010: Origin and fate of atmospheric moisture over continents. *Water Resour. Res.*, **46**, W09525, <https://doi.org/10.1029/2010WR009127>.
- Wang, C., F. Kucharski, R. Barimalala, and A. Bracco, 2009: Teleconnections of the tropical Atlantic to the tropical Indian and Pacific Oceans: A review of recent findings. *Meteor. Z.*, **18**, 445–454, <https://doi.org/10.1127/0941-2948/2009/0394>.
- Wang, J., B. Yang, and F. C. Ljungqvist, 2015: A millennial summer temperature reconstruction for the eastern Tibetan Plateau from tree-ring width. *J. Climate*, **28**, 5289–5304, <https://doi.org/10.1175/JCLI-D-14-00738.1>.
- , —, —, J. Luterbacher, T. J. Osborn, K. R. Briffa, and E. Zorita, 2017: Internal and external forcing of multidecadal Atlantic climate variability over the past 1,200 years. *Nat. Geosci.*, **10**, 512–517, <https://doi.org/10.1038/ngeo2962>.
- Xie, H., J. Ye, X. Liu, and E. Chongyi, 2010: Warming and drying trends on the Tibetan Plateau (1971–2005). *Theor. Appl. Climatol.*, **101**, 241–253, <https://doi.org/10.1007/s00704-009-0215-9>.
- Yang, K., H. Wu, J. Qin, C. Lin, W. Tang, and Y. Chen, 2014: Recent climate changes over the Tibetan Plateau and their impacts on energy and water cycle: A review. *Global Planet. Change*, **112**, 79–91, <https://doi.org/10.1016/j.gloplacha.2013.12.001>.
- Yao, Q. C., and Coauthors, 2017: Pacific–Atlantic Ocean influence on wildfires in northeast China (1774 to 2010). *Geophys. Res. Lett.*, **44**, 1025–1033, <https://doi.org/10.1002/2016GL071821>.
- Yao, T. D., and Coauthors, 2012: Different glacier status with atmospheric circulations in Tibetan Plateau and surroundings. *Nat. Climate Change*, **2**, 663–667, <https://doi.org/10.1038/nclimate1580>.
- , and Coauthors, 2013: A review of climatic controls on  $\delta^{18}\text{O}$  in precipitation over the Tibetan Plateau: Observations and simulations. *Rev. Geophys.*, **51**, 525–548, <https://doi.org/10.1002/rog.20023>.
- You, Q., S. Kang, N. Pepin, and Y. Yan, 2008: Relationship between trends in temperature extremes and elevation in the eastern and central Tibetan Plateau, 1961–2005. *Geophys. Res. Lett.*, **35**, L04704, <https://doi.org/10.1029/2007GL032669>.
- , J. Min, and S. Kang, 2016: Rapid warming in the Tibetan Plateau from observations and CMIP5 models in recent decades. *Int. J. Climatol.*, **36**, 2660–2670, <https://doi.org/10.1002/joc.4520>.
- , Z. H. Jiang, G. W. K. Moore, Y. T. Bao, L. Kong, and S. C. Kang, 2017: Revisiting the relationship between observed warming and surface pressure in the Tibetan Plateau. *J. Climate*, **30**, 1721–1737, <https://doi.org/10.1175/JCLI-D-15-0834.1>.
- Zhang, R., T. L. Delworth, and I. M. Held, 2007: Can the Atlantic Ocean drive the observed multidecadal variability in Northern Hemisphere mean temperature? *Geophys. Res. Lett.*, **34**, L02709, <https://doi.org/10.1029/2006GL028683>.